RSC Advances

COMMUNICATION

View Article Online
View Journal | View Issue

Cite this: *RSC Adv.*, 2014, **4**, 57743

Received 24th August 2014
Accepted 27th October 2014

DOI: 10.1039/c4ra09170a

www.rsc.org/advances

Sensitive and easily recyclable plasmonic SERS substrate based on Ag nanowires in mesoporous silica†

Xuefeng Yan,[a] Lingzhi Wang,*[a] Dianyu Qi,[a] Juying Lei,[a] Bin Shen,[a] Tapas Sen*[b] and Jinlong Zhang*[a]

Ag nanowires confined in mesoporous SBA-15 show improved SERS activity towards organics detection compared with Ag nanospheres. The mild chemical transformation reaction between Ag and AgCl and photocatalytic elimination of analyte were utilized to recycle the SERS detection.

Surface-enhanced Raman scattering (SERS) is a strong technique for rapid and sensitive detection of biomolecules, water pollutants and monitoring of chemical reactions.[1] Noble metals such as Ag, Au and Cu are the most commonly used SERS substrates.[2] Among them, Ag has received most attention mainly attributed to its strong surface plasmon polarization mode in visible light range. By appropriately controlling gap distance between neighbouring Ag nanoparticles (NPs), single-molecule detection sensitivity can even be achieved due to formation of hot spot with high electromagnetic enhancement in the gap.[3] However, as commonly found from other nanometre-sized metal particles, Ag NPs have strong tendency to aggregate in an uncontrollable way during storage, which leads to low detection reproducibility and reliability. The common method for achieving reliable detection is adopting freshly-made Ag NPs for each-time detection, which is ineffective and uneconomic especially in the case of large-scale detection. Therefore, preparation of SERS substrate with long stability and recyclability besides sensitivity is essential for wide application of SERS detection in different fields.

Some methods have been developed for preventing noble metal NPs from aggregation, where adoption of polymer or surfactant as capping agent, and coating metal NPs with inert shell have proven to be efficient for stabilization.[4] However, some undesirable side effects as well as requirements for high synthesis techniques have severely restricted wide application of above routes. For examples, analyte may be screened by capping agent due to electrostatic or hydrophobic repulsion, leading to interference on detection accuracy. Coating Ag with super-thin and chemically inert silica shell may improve both stability and sensitivity when hot spots are produced from gaps between dimers. However, rigorous synthesis requirement on uniform production of dimers with appropriately thin shell thickness weakens the application feasibility.[5] Besides capping or coating, other ways such as encapsulating metal NPs in porous matrix have also proven effective in preventing particles from severe agglomeration.[6] Moreover, compared with efforts on improving stability, current researches pay less attention on acquiring recyclability of plasmon type SERS substrates due to lacking of efficient method. The combination of semiconductor photocatalyst and metal NP is the most popularly substituent way for recycling of SERS substrate through photocatalytic elimination of organic analyte.[7]

Among various porous structures, mesoporous silica has recently drawn most attention as carrier due to its long-range ordered pore channel and various pore structures.[8] Currently, Ag NPs have been successfully fabricated through methods including thermal decomposition,[6c] photo-illumination[9] and microwave-heating.[10] Some unique advantages have been revealed from mesoporous silica confined Ag NP as SERS substrate besides improved stability. The most immediate one is it can achieve selective detection of analytes through size-screening effect of porous system.[11] Moreover, the uniform and parallel pore channel offers advantages such as controlled diameter, morphology and density of NPs inside pores and thus, the gaps between them, which are helpful to improve the detection sensitivity by generating hot spots. It is desirable a high-density and uniform loading of metal NPs with large size can be achieved to produce enough hot spots with strong local electric field, which is however contradicted with the preservation of pore ordering. The unavoidable situation is mesoporous

[a]*Key Lab for Advanced Materials and Institute of Fine Chemicals, East China University of Science and Technology, Meilong Road 130, Xuhui District, Shanghai, 200237, P. R. China. E-mail: wlz@ecust.edu.cn; jizhang@ecust.edu.cn*

[b]*Centre for Materials Science, Institute of Nanotechnology and Bioengineering, School of Forensic and Investigative Sciences, University of CentralLancashire, Preston, UK. E-mail: TSen@uclan.ac.uk*

† Electronic supplementary information (ESI) available. See DOI: 10.1039/c4ra09170a

system may be deteriorated due to the excessive introduction of Ag NPs, leading to poor accessibility of SERS active particle. Another unneglectable problem is that the restricted growth of Ag particle may decrease the plasmon effect, which is why SERS detection performance of Ag NPs dispersed in mesoporous silica matrix has been long ignored compared with their catalysis performance.

Here, SBA-15 loaded with Ag nanospheres (Ag SBA-15/NS) and nanowires (Ag SBA-15/NW) were respectively fabricated and the SERS activities were studied by using MB as target analyte. The interference of Ag content is excluded since NSs are transformed from NWs through *in situ* high-temperature treatment. Highly sensitive SERS detection sensitivity on the order of 10^{-8} M is achieved from Ag NWs parallel aligned and high-density distributed in SBA-15. This SERS substrate has a good detection stability after long-time storage (7 days) without any protecting from light illumination. Moreover, organic analyte can be quickly photocatalytically eliminated by AgCl within 10 minutes, which is transformed from Ag through a mild reaction with $FeCl_3$. More interestingly, SERS activity can be simultaneously regenerated through photo-reduction of AgCl during the photocatalytic elimination process of MB. Such an ingeniously reversible transformation process makes the SERS detection easily recyclable.

Ag SBA-15/NW was prepared through two-solvent nanocasting of $AgNO_3$ in the pore channel, followed by a pyrolysis treatment at 350 °C for 2 h. Ag SBA-15/NS was transformed from Ag SBA-15/NW by a further calcination treatment at 550 °C for another 2 h.[6c] Both of NWs and NSs are highly dispersed in the pore channels of SBA-15 as verified by transmission electron microscope (TEM) (Fig. 1). Ag NSs have particle size of 40 ± 10 nm and most of NWs have length of about 80 ± 10 nm. Ag NWs are parallel aligned to each other by duplicating the parallel arranged pore channels of mesoporous matrix and the density of Ag NWs is higher than that of NSs. Moreover, most of meosporous channels in samples Ag SBA-15/NW and Ag SBA-15/NS are still well preserved and highly accessible. Wide-angle XRD patterns of AG NWs and NSs show well-resolved peaks at $2\theta = 38.0°$, 44.3°, 64.5°, and 77.3°, which are attributed to (111), (200), (220), and (311) reflections of Ag with cubic asymmetry. The stronger peak intensity of Ag NS than NW indicates the higher crystallinity, which should be attributed to the higher-temperature calcination treatment.

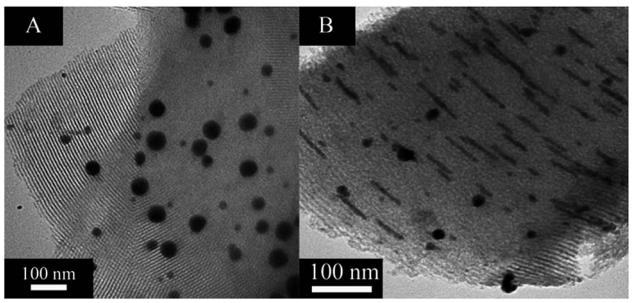

Fig. 1 TEM images of (A) Ag SBA-15/NS and (B) Ag SBA-15/NW.

Small-angle X-ray diffraction (XRD) patterns of SBA-15, Ag SBA-15/NS and Ag SBA-15/NW clearly indicate that mesoporous structure can be still remained after the encapsulation of Ag NSs or NWs (Fig. 2). However, the pore ordering is partly deteriorated as observed from the decreased peak intensity. The nitrogen adsorption-desorption isotherms of SBA-15, Ag SBA-15/NS and Ag SBA-15/NW all show typical type IV curves with H2 hysteresis loop (Fig. S1†), verifying the preservation of mesoporous structure in the presence of Ag NPs. The BET surface area of SBA-15 is 627.5 $m^2 g^{-1}$, which decreases to 451.2 $m^2 g^{-1}$ and 358.1 $m^2 g^{-1}$ for Ag SBA-15/NS and Ag SBA-15/NW, respectively. Meanwhile, the pore volume of SBA-15 also decreases from 0.73 $cm^3 g^{-1}$ to 0.60 $cm^3 g^{-1}$ and 0.61 $cm^3 g^{-1}$ for Ag SBA-15/NS and Ag SBA-15/NW. The decreased specific surface area and pore volume are attributed to the part occupation of pore channel by Ag NPs, which inevitably sacrifices the pore accessibility. The specific surface area of Ag SBA-15/NW is more decreased than that of SBA-15/NS due to more occupation of pore channel by higher-density distributed Ag NWs.

UV-Vis diffuse reflection spectra show that Ag SBA-15/NW has a wider and stronger absorption band than that of Ag SBA-15/NS centered at 400 nm (Fig. 3). The peak below 300 nm

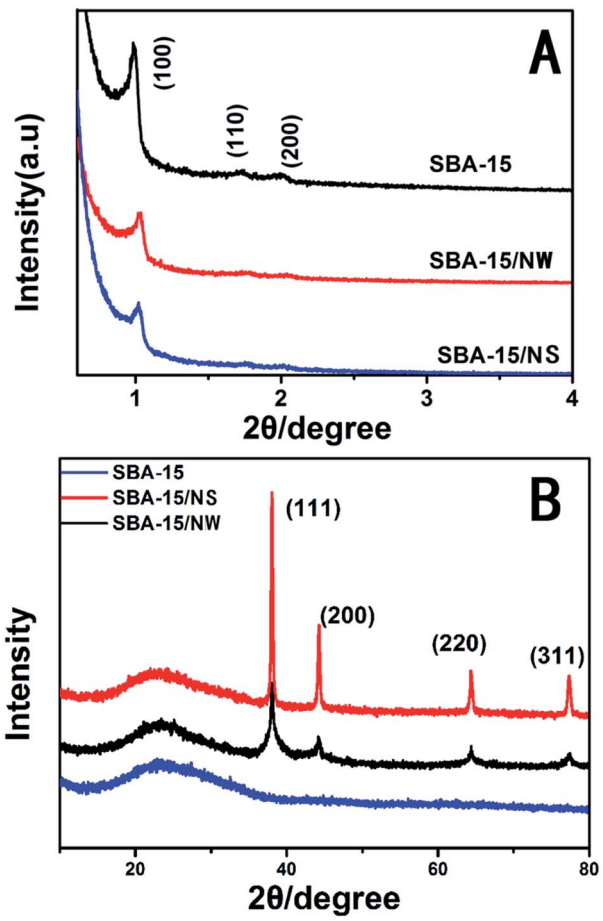

Fig. 2 (A) Small-angle pattern of SBA-15, Ag SBA-15/NS and Ag SBA-15/NW; (B) wide-angle XRD patterns of SBA-15, Ag SBA-15/NS and Ag SBA-15/NW.

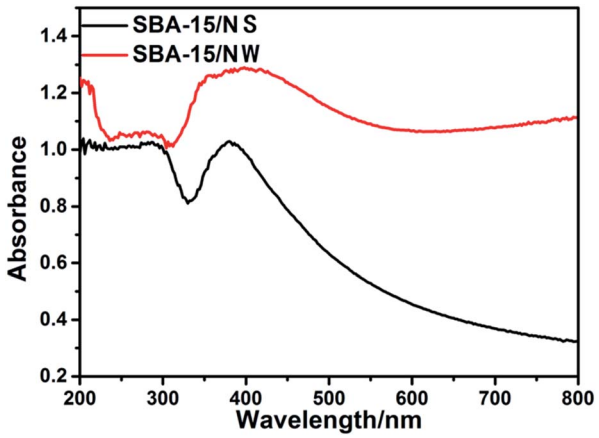

Fig. 3 UV-Vis diffuse reflection spectra of Ag SBA-15/NS and Ag SBA-15/NW composites.

is attributed to the absorption of SiO_2 matrix. The band at around 400 nm is characteristic absorption of spherical Ag NP. It is known that new absorption band can be formed at longer-wavelength region for nonspherical NPs such as nanorod and nanowire, and the intensity ratio between the peaks at longer and shorter wavelength regions increases with the increasing length/diameter ratio. Therefore, the widened absorption in the long-wavelength range observed from Ag SBA-15/NW is attributed to the longer length/diameter ratio of Ag NWs. The higher peak intensity of Ag NWs indicates the formation of a stronger local electric field compared with that of Ag NSs.

The SERS activity was investigated by first adopting MB as a model. Obvious Raman signals featuring the peak at 1618 cm^{-1} is observed from Ag SBA-15/NS when the concentration of MB is 10^{-4} M. The signal is significantly decreased at 10^{-5} M, which keeps decreasing at 10^{-6} M and completely disappears at 10^{-7} M (Fig. 4A). Whilst the signal from Ag SBA-15/NW is still distinct and not much decreased at 10^{-7} M, which is still observable when the concentration of MB decreases to 5×10^{-8} M and does not completely disappear until the concentration decreases to 10^{-8} M. It is expected that the sensitivity should be further optimized by tuning the density or length/diameter ratio of Ag NW. However, our preliminary study on increasing the Ag density does not leads to qualitative improvement on detection sensitivity (Fig. 5). Further tuning about structure parameter will be carried in our lab to explore more optimum detection sensitivity. Besides MB, we also applied Ag SBA-15/NW for the detection of some other organics like atrazine, p-nitrophenol and p-aminophenol, and also obtained well-resolved Raman signals (Fig. S2†), implying Ag SBA-15/NW presented here is indeed applicable for the SERS detection of different analytes.

Based on the above results, the higher sensitivity of Ag NWs than that of Ag NSs encapsulated in SBA-15 is discussed as follows. As verified by the TEM images, Ag NWs are more closely packed than those of Ag NSs with the same loading amount in per unit area of silica matrix. The uniform and parallel distribution of high-density Ag NWs is advantageous to generate stronger local electric field due to coupling effect between

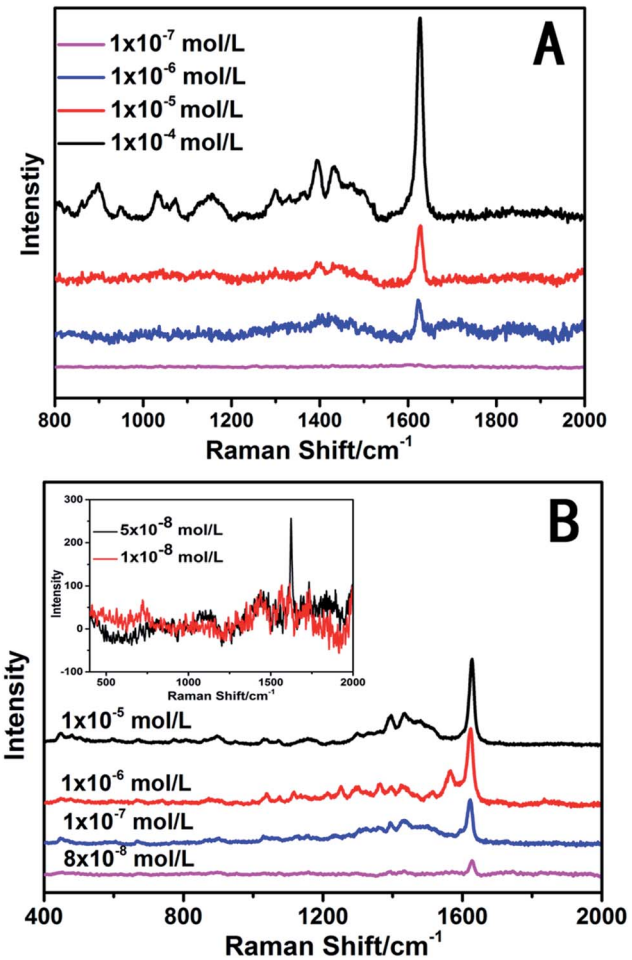

Fig. 4 Raman spectra of MB with different concentrations from (A) Ag SBA-15/NS and (B) Ag SBA-15/NW.

neighbouring plasmonic sites, which can form stronger electromagnetic enhancement effect for SERS analysis under laser illumination. Moreover, the neighbouring pore channels of SBA-15 are actually interconnected through micropores in the pore framework ($S_{mic} = 25$ m^2 g^{-1}). Therefore, large amount of surface sites of Ag NWs encapsulated in the pore channel is actually still exposed and accessible to analyte molecule. Ag NSs are transformed from the agglomeration of NWs through high-temperature treatment, which has lower specific surface sites. The distance between Ag NSs is larger than that between Ag

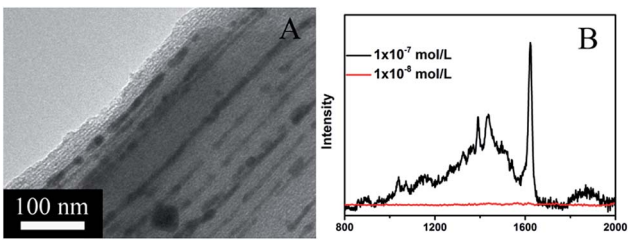

Fig. 5 (A) TEM of Ag SBA-15/NW with increased silver content and (B) Raman spectra of MB with concentrations of 10^{-7} M and 10^{-8} M.

NWs, decreasing the coupling interaction between neighbouring NSs. The stronger local electric field and more accessible surface sites ultimately lead to the improved SERS signal of MB from Ag NWs. It is expected that the sensitivity can be further increased by increasing the density or tuning the length/diameter ratio of Ag NWs. However, the tuning should be finely optimized to avoid poor deterioration and blockage.

Besides sensitivity, the stability of Ag NWs in SBA-15 was also tested by comparing the detection performance of Ag SBA-15/NW for MB before and after one-week preservation without any protection from light illumination. The result indicates distinct peaks from MB can still be observed after long-time storage (Fig. 6). In comparison, Ag NPs with size of 50 nm and stored in water finally precipitated from solution during storage, which should be ascribed to significant particle-agglomeration. The stabilization of Ag NWs encapsulated in SBA-15 should be ascribed to the fixing effect of nanometre-sized rigid pore channels. The good stability of Ag SBA-15/NW together with high sensitivity well illustrates its priority as a SERS substrate.

Ag SBA-15/NW can be recycled by eluting MB with ethanol after performing Raman analysis (Fig. S3†). The detection performance can be preserved for 3 cycles. However, it is more desirable if the adsorbed organics can be harmlessly eliminated through means such as photocatalysis. In fact, photocatalytic renewing of SERS substrate have been commonly adopted by semiconductor-containing SERS substrate.[12] Ag can be oxidized to AgCl, an intensively studied semiconductor photocatalyst in recent years.[13] Meanwhile, the photo-induced reduction of AgCl to Ag (photo-corrosion) has been commonly observed during photocatalysis process, which is generally undesirable for photocatalyst. However, we here ingeniously utilize the mildly convertible reaction between Ag and AgCl to achieve a recyclable SERS detection system with the aid of photocatalysis. We first adopt $FeCl_3$ as the oxidant to transform Ag NWs to AgCl after the detection of MB by simply dropwise adding appropriate amount of $FeCl_3$ solution on Ag SBA-15/NW film. The driving force for this reaction relies on the reduced standard reduction potential of Ag couples from +0.80 V (*vs.* SHE for Ag^+/Ag pair) to +0.223 V (*vs.* SHE for AgCl/Ag pair), which is lower than that of +0.771 V (*vs.* SHE for Fe^{3+}/Fe^{2+} pair).[14] Wide-angle XRD pattern (Fig. 7, red line) exhibits diffraction peaks at $2\theta = 27.8°$, 32.2°, 46.2°, 54.8°, 57.5° and 76.7° for the sample after treated with $FeCl_3$, which are associated with (111), (200), (220), (311), (222) and (420) reflections of AgCl. A weak peak around $2\theta = 38.2°$ ascribed to the cubic phase of Ag (111) can also been observed, indicating Ag and AgCl are co-existed in the pore channel. Previous report on the oxidation of Ag nanorod with $FeCl_3$ indicates that Ag is coated by AgCl in a core@shell form.[14] Here, the combination form of Ag and AgCl in the pore channel is hardly resolvable due to the small diameter. However, since SBA-15 we used has microporous framework, $FeCl_3$ can still approach to different surface sites of Ag through the micropores in the framework. Therefore, it is quite possible that Ag should also be coated by AgCl in the core@shell form (Ag@AgCl SBA-15/NW) after the reaction.

The SERS signals of MB (10^{-5} M) from Ag@AgCl SBA-15/NW before photocatalysis treatment becomes weak but is still observable (not shown), indicating Ag@AgCl SBA-15/NW still preserve the SERS activity. All of the signals completely disappear after ten-minute *in situ* illumination. The photocatalytic degradation is consistent with first-order reaction kinetic model as verified from a proportionally enlarged photocatalysis system (Fig. S4†). After the photocatalysis process, re-adsorption of MB was carried out and the Raman signals of MB with intensity comparable to that from Ag SBA-15/NW can be obtained, which can be eliminated again by another illumination treatment. The whole detection-elimination process can be well reproduced for 3 cycles (Fig. 8). The wide-angle XRD pattern indicates the peak at 38.2° increases after the photocatalysis process (Fig. 7, black line), indicating part of AgCl is photo-reduced back to Ag. So, the recovered peak intensity should be ascribed to the part recovery of Ag from AgCl. Long-time illumination (10 h) leads to

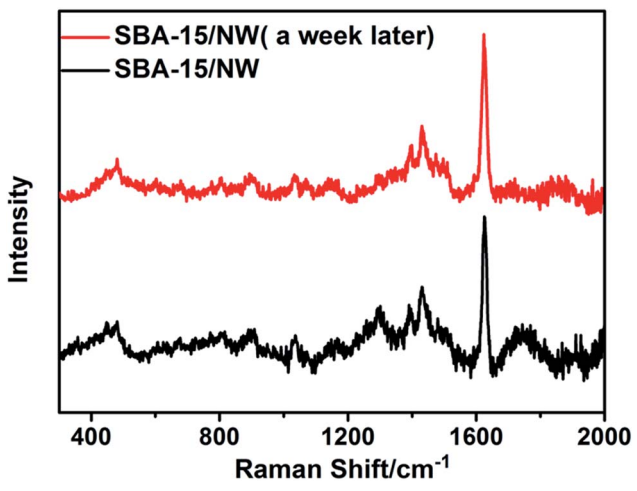

Fig. 6 SERS spectra of 10^{-5} M MB obtained from Ag SBA-15/NW after one-week storage without any protection from light illumination.

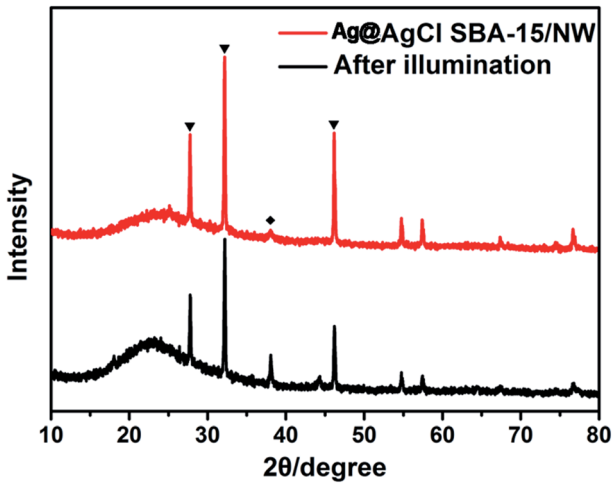

Fig. 7 Wide-angle XRD patterns of Ag@AgCl SBA-15/NW before and after photocatalysis illumination. Triangle and square represent AgCl and Ag, respectively.

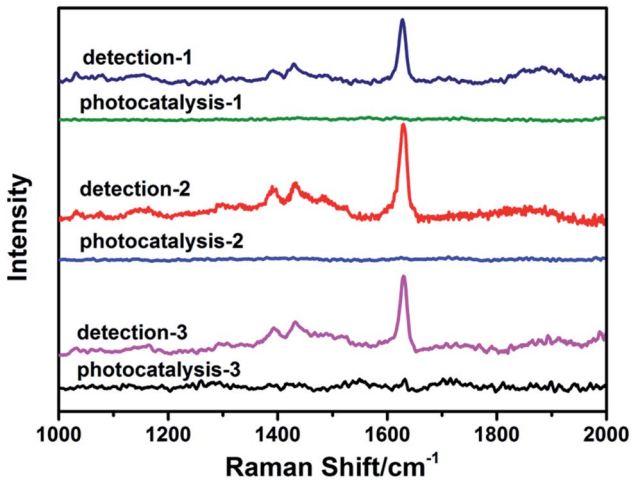

Fig. 8 SERS detection performance of Ag SBA-15/NW on 10^{-5} mol L^{-1} MB after three recycles treated by photocatalysis.

the continuous increasing of Ag amount (Fig. S5†). The above results illustrate the SERS detection should be further recyclable by accordingly controlling the transformation orientation of the mildly reversible reaction between Ag and AgCl.

Conclusions

In conclusion, the SERS detection sensitivities of SBA-15 confined Ag NWs and NSs with the same loading amount were compared by using MB as the analyte, where Ag NWs show higher sensitivity than Ag NSs due to more accessible surface sites and stronger local electric field caused by high-density distribution and parallel alignment. The SERS detection can be repeatedly recycled by utilizing the mildly reversible transformation reaction between Ag and AgCl and the photocatalytic elimination of organic analyte after each detection, which demonstrates a feasible way for design and fabrication of recyclable plasmonic SERS substrate.

Acknowledgements

This work has been supported by the National Nature Science Foundation of China (21173077 and 21377038), the National Basic Research Program of China (973 Program, 2013CB632403), the Science and Technology Commission of Shanghai Municipality (14ZR1410700, 14230710500, 12230705000 and 12XD140220), the Research Fund for the Doctoral Program of Higher Education (20120074130001) and the Fundamental Research Funds for the Central Universities.

Notes and references

1 (*a*) D. L. Jeanmaire and R. P. Van Duyne, *J. Electroanal. Chem.*, 1977, **84**(1), 1–20; (*b*) M. G. Albrecht and J. A. Creighton, *J. Am. Chem. Soc.*, 1977, **99**(15), 5215–5217.

2 (*a*) C. B. Gao, Y. X. Hu, M. S. Wang, M. F. Chi and Y. D. Yin, *J. Am. Chem. Soc.*, 2014, **136**, 7474–7479; (*b*) M. S. Wang, C. B. Gao, L. He, Q. P. Lu, J. Z. Zhang, C. Tang, S. Zorba and Y. D. Yin, *J. Am. Chem. Soc.*, 2013, **135**, 15302–15305; (*c*) L. Chen, J. Yu, T. Fujita and M. Chen, *Adv. Funct. Mater.*, 2009, **19**, 1221–1226; (*d*) C. C. Kong, J. Lv, S. D. Sun, X. P. Song and Z. M. Yang, *RSC Adv.*, 2014, **4**, 27074–27077.

3 (*a*) K. Kneipp, Y. Wang, H. Kneipp, L. T. Perelman, I. Itzkan, R. R. Dasari and M. S. Feld, *Phys. Rev. Lett.*, 1997, **78**(9), 1667–1670; (*b*) S. Nie and S. R. Emory, *Science*, 1997, **275**(5303), 1102–1106; (*c*) P. H. C. Camargo, M. Rycenga, L. Au and Y. N. Xia, *Angew. Chem., Int. Ed.*, 2009, **48**, 2180–2184; (*d*) J. P. Camden, J. A. Dieringer, Y. M. Wang, D. J. Masiello, L. D. Marks, G. C. Schatz and R. P. Van Duyne, *J. Am. Chem. Soc.*, 2008, **130**, 12616–12617; (*e*) S. Tokonami, K. Nishida, Y. Nishimura, S. Hidaka, Y. Yamamoto, H. Nakao and T. Lida, *Res. Chem. Intermed.*, 2014, **40**, 2337–2346; (*f*) M.-C. Wu, M.-P. Lin and S.-W. Chen, *RSC Adv.*, 2014, **4**, 10043–10050.

4 (*a*) X. M. Qian, J. Li and S. M. Nie, *J. Am. Chem. Soc.*, 2009, **131**, 7540–7541; (*b*) R. A. Álvarez-Puebla, R. Contreras-Cáceres, I. Pastoriza-Santos, J. Pérez-Juste and L. M. Liz-Marzán, *Angew. Chem., Int. Ed.*, 2009, **48**, 138–143; (*c*) B. Küstner, M. Gellner, M. Schütz, F. Schöppler, A. Marx, P. Ströbel, P. Adam, C. Schmuck and S. Schlücker, *Angew. Chem., Int. Ed.*, 2009, **48**, 1950–1953.

5 (*a*) K. L. Wustholz, A. Henry, J. M. McMahon, R. G. Freeman, N. Valley, M. E. Piotti, M. J. Natan, G. C. Schatz and R. P. Van Duyne, *J. Am. Chem. Soc.*, 2010, **132**, 10903–10910; (*b*) A. Kudelski and S. Wojtysiak, *J. Phys. Chem. C*, 2012, **116**, 16167–16174; (*c*) M. Shanthil, R. Thomas, R. S. Swathi and K. G. Thomas, *J. Phys. Chem. Lett.*, 2012, **3**, 1459–1464.

6 (*a*) Y. J. Han, J. M. Kim and G. D. Stucky, *Chem. Mater.*, 2000, **12**, 2068–2069; (*b*) F. Kleitz, S. H. Choi and R. Ryoo, *Chem. Commun.*, 2003, 2136–2137; (*c*) X. Huang, W. J. Dong, G. Wang, M. Yang, L. Tan, Y. H. Feng and X. X. Zhang, *J. Colloid Interface Sci.*, 2011, **359**, 40–46; (*d*) J. Zhu, Z. Konya, V. F. Puntes, I. Kiricsi, C. X. Miao, J. W. Ager, A. P. Alivisatos and G. A. Somorjai, *Langmuir*, 2003, **19**, 4396–4401.

7 (*a*) E.-Z. Tan, P.-G. Yin, T.-t. You, H. Wang and L. Guo, *ACS Appl. Mater. Interfaces*, 2012, **4**, 3432–3437; (*b*) X. Jiang, X. Li, H. Hu, D. Li, Z. Shen, Q. Xiong, S. Li and H. J. Fan, *ACS Appl. Mater. Interfaces*, 2012, **4**, 2180–2185.

8 (*a*) C. T. Kresge, M. E. Leonowicz, W. J. Roth, J. C. Vartuli and J. S. Beck, *Nature*, 1992, **359**(6397), 710–712; (*b*) D. Zhao, J. Feng, Q. Huo, N. Melosh, G. H. Fredrickson, B. F. Chmelka and G. D. Stucky, *Science*, 1998, **279**, 548–552.

9 A. Fukuoka, H. Araki, J. Kimura, Y. Sakamoto, T. Higuchi, N. Sugimoto, S. Inagaki and M. Ichikawa, *J. Mater. Chem.*, 2004, **14**, 752–756.

10 K. Fuku, R. Hayashi, S. Takakura, T. Kamegawa, K. Mori and H. Yamashita, *Angew. Chem., Int. Ed.*, 2013, **52**, 7446–7450.

11 V. López-Puente, S. Abalde-Cela, P. C. Angelomé, R. A. Alvarez-Puebla and L. M. Liz-Marzán, *J. Phys. Chem. Lett.*, 2013, **4**, 2715–2720.

12 (*a*) D. Y. Qi, L. L. Liu, L. Z. Wang and J. L. Zhang, *J. Am. Chem. Soc.*, 2014, **136**, 9886–9889; (*b*) X. Jiang, X. Li, X. Jia, G. Li,

X. Wang, G. Wang, Z. Li, L. Yang and B. Zhao, *J. Phys. Chem. C*, 2012, **116**, 14650.

13 (*a*) P. Wang, B. B. Huang, X. Y. Qin, X. Y. Zhang, Y. Dai, J. Y. Wei and M.-H. Whangbo, *Angew. Chem., Int. Ed.*, 2008, **47**, 7931–7933; (*b*) P. Wang, B. B. Huang, Z. Z. Lou, X. Y. Zhang, X. Y. Qin, Y. Dai, Z. K. Zheng and X. N. Wang, *Chem.–Eur. J.*, 2010, **16**, 538–544.

14 (*a*) Y. P. Bi and J. H. Ye, *Chem. Commun.*, 2009, 6551–6553; (*b*) Y. G. Sun, *J. Phys. Chem. C*, 2010, **114**, 2127–2133.